Meteoritics 27, 361–370 (1992)

Dissemination and fractionation of projectile materials in the impact melts from Wabar Crater, Saudi Arabia

DAVID W. MITTLEFEHLDT,[1] THOMAS H. SEE[1] AND FRIEDRICH HÖRZ[2]
[1]Lockheed ESC, C23, 2400 Nasa Road 1, Houston, Texas 77058, USA
[2]Solar System Exploration Division, SN2 NASA-Johnson Space Center, Houston, Texas 77058, USA

(*Received 1991 October 10; accepted in revised form 1992 May 10*)

Abstract—We have analyzed small, ballistically dispersed melt samples in the form of aerodynamically shaped spheres, dumbbells, teardrops, *etc.*, from Wabar Crater, Saudi Arabia, and have compared these to our previous study of the more massive, black and white melt specimens. The smaller melt samples differ from the more massive melts in that they are petrographically and chemically more homogeneous, possess fewer, more diffuse schlieren and contain much less clastic detritus. These observations suggest higher peak temperatures for the smaller melt samples than for the massive black and white melts which represent Wabar's major melt-zone.

Analyses of the Wabar and Nejed (paired with Wabar) meteorites permit detailed comparison of the unaltered projectile with impactor residues in the melts. Siderophile element concentrations indicate that the small glass beads commonly contain >10% meteoritic component, compared to <5% for the massive black and white melts. One glass bead was found to contain ~17% meteoritic component. Based on models for melt production during cratering, we deduce that more meteoritic material was mixed with the upper stratigraphic horizons of Wabar's melt zone than with the lower parts. Siderophile elements in all Wabar melt specimens are fractionated relative to the Wabar-Nejed meteorite and have Fe/Ni ratios up to ~1.8 times that of Wabar-Nejed for the most siderophile element-rich glasses. The abundance sequence of siderophiles in the melts relative to the projectile is Fe ≈ Co > Ni ≈ Ir ≈ As ≫ Au. Although this sequence seems incompatible with *simple* vapor fractionation of either elements or oxides, we believe that a *complex* vapor fractionation process most likely produced the observed siderophile element abundances.

Our sample suite should be representative of all materials found in and around the Wabar structure, and we conclude that substantial quantities of the projectile were lost to the atmosphere, most likely as vapor. No fractionation of lithophile elements is observed in the glasses relative to the target rocks. Although fractionation of the impactor must have occurred prior to intimate mixing of projectile and target, details of the actual fractionation mechanism(s) remain poorly understood. The results of this study indicate that caution is necessary when attempting to define impactor types and masses from compositional data for impact melts from other craters.

INTRODUCTION

THE WABAR CRATERS OF CENTRAL SAUDI ARABIA were formed ~6400 years ago (Storzer and Wagner, 1977), when a IIIA iron meteorite impacted a quartz dominated target. The exact stratigraphy of the target is not known and questions remain whether the loosely consolidated sandstone(s) were covered by a thin veneer of drift sand at the time of impact (Philby, 1933; Spencer, 1933a). Early observers reported the presence of a number of craters, the largest measuring 90 m in diameter. All samples in this study originated from this large crater because the smaller structures were inundated by drift sand before Holm and Barnes collected a large suite of samples (Holm, 1962). These samples, for the most part, reside at the Smithsonian Institution (Washington, D.C.), which generously provided all samples used in this investigation. The Wabar and Nejed (paired with Wabar) meteorites represent fragments of the impactor found in the general vicinity of, yet not directly at, the impact site (Buchwald, 1975). Thus, the initial conditions of the Wabar impact may be reconstructed in unusual detail: specimens of the impactor are available, the target is relatively simple lithologically and compositionally, and a variety of impact products have been collected in the field for detailed investigations.

Petrographic and geochemical studies indicate that all displaced materials, especially the melts, are of an exceptionally pristine and unweathered nature (Spencer, 1933b; Ehmann, 1962; Brett, 1967; Morgan *et al.*, 1975; Gibbons *et al.*, 1976; Hörz *et al.*, 1989), thereby eliminating some problems related to secondary processes which frequently complicate analysis and interpretation of siderophile elements in many terrestrial impact melts (*e.g.*, Palme, 1982). Hörz *et al.* (1989) presented petrographic and compositional analyses of the black and white impact melts from Wabar, thus augmenting the initial observations of Spencer (1933b) and those of Brett (1967). These melts occur as massive, highly vesicular chunks inside the crater and were interpreted as representing the main melt zone of the Wabar impact (Hörz *et al.*, 1989). Because of the crater's relatively small size, the melts did not pool on the crater bottom to form a contiguous melt sheet characteristic of large impact structures. The black and white melts contained, on average, ~4% and ~0.5% meteoritic contamination, respectively, which lead to the conclusion that projectile dissemination can be heterogeneous within the melt zone of a single crater (Hörz *et al.*, 1989).

The present study concentrates on the analysis of small melt samples found as droplets, spheres, dumbbells and their fragments, generally <1 cm in size, and seemingly abundant on the crater rim (Spencer, 1933b). The objective of this sample selection was to analyze only materials that demonstrably underwent ballistic transport. Therefore, care was exercised to include only specimens that possessed shapes or other morphological properties indicative of surface tension, thereby indicating free-flight during ballistic transport for the samples. Such ballistically dispersed materials contrast with mechanical-erosion products of the more massive melts which generally occur as angular chips and fragments, and which constitute as much as 4% by volume of the surface samples at the Wabar site (Hörz *et al.*, 1989). The absolute abundance of the ballistic melt-spray is not known precisely, yet field descriptions suggest that they are fairly abundant.

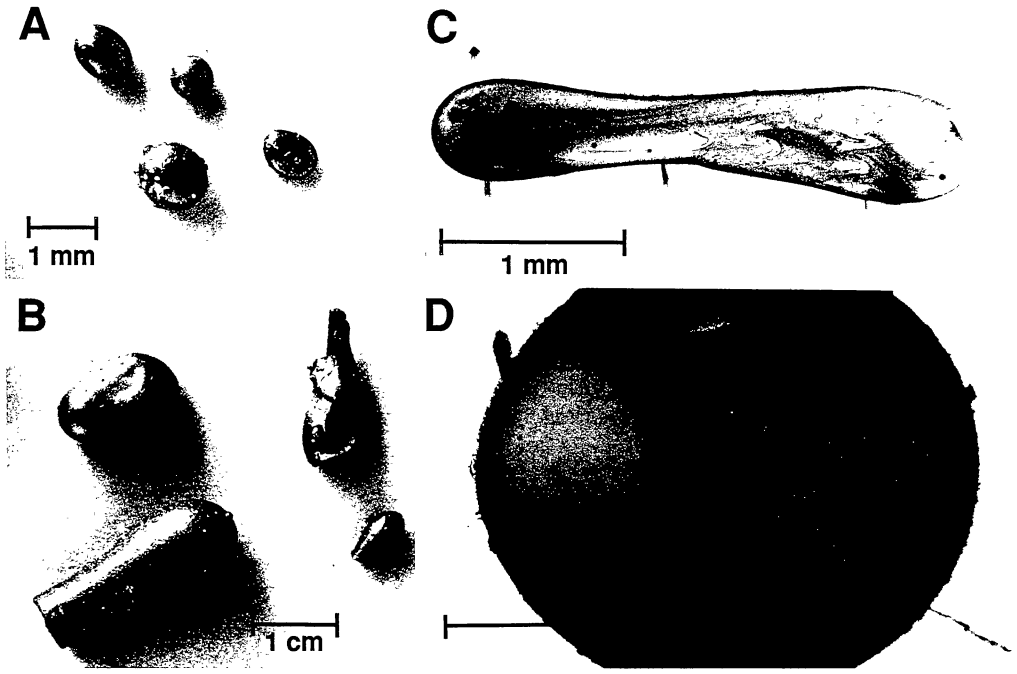

FIG. 1. Representative melt-spray samples from Wabar Crater, Saudi Arabia. Typical shapes of small beads (A) and large beads (B). Typical thin-section appearance of a small bead dumbbell (C) and sphere (D). Note the relatively faint schlieren and relative paucity of clastic debris.

Experiments (Stöffler *et al.*, 1975), terrestrial observations (Grieve, 1982) and theory (*e.g.*, Ahrens and O'Keefe, 1977; Maxwell, 1977) indicate that ballistic ejecta are derived from higher stratigraphic horizons than materials that remain inside a crater. Therefore, the melt-spray samples investigated in this report are assumed to have been derived from a location stratigraphically higher than those that yielded the more massive black and white melts. The upper level of the target zone is expected to experience higher shock stresses and temperatures, and to be physically closer to the penetrating meteorite, leading to increased contamination by meteoritic materials.

Following our analysis of numerous, ballistic melt samples, it became necessary to obtain internally self-consistent, systematic compositional information pertaining to the Wabar projectile itself. Therefore, we obtained samples of the Wabar and Nejed meteorites which were kindly analyzed by J. T. Wasson. Throughout this report, "Wabar meteorite" will refer to both Wabar and Nejed.

SAMPLE MATERIALS AND ANALYTICAL METHODS

All melt samples were selected by one of us (F.H.) from the collection of the Smithsonian Institution, through the courtesy of R. Clarke and K. Fredriksson. Of the many specimens comprising this collection, only samples for which the assumption of ballistic transport and free-flight appeared reasonable were selected (Fig. 1). Selection concentrated on spheres, dumbbells, teardrops and ellipsoidal objects ranging in size from less than a millimeter to several centimeters, which spanned the available size-range of the Smithsonian suite. Careful screening of the entire collection established that all free-flight objects >1 mm were of the dark-melt variety. A single transparent sphere (<0.5 mm), which may be the equivalent of the massive white melts, was observed among the objects.

Due to vastly differing masses of individual specimens, it was necessary to devise different procedures in the preparation of various aliquots for chemical and petrographic analysis. Objects that were sufficiently large (>1 mm) were physically split by gently breaking them into a few large fragments. One aliquot was used for thin sectioning and subsequent electron-microprobe investigations, while the other was prepared for instrumental neutron activation analysis (INAA). One vial contained numerous beads <1 mm in diameter. Several of these beads were selected for electron-microprobe analysis, and the rest were grouped into one INAA sample. After the normal INAA counting schedule, the 16 beads in this grouped sample were separated and individually counted for the long-lived radioisotopes of Fe, Sc, Cr, Co, Ni and Ir in order to obtain some measure of intersample variability. The averages of these data, weighted according to bead mass, agree well with the INAA data on the grouped sample. Subsequently, several of these radioactive beads were made into thin sections for electron-microprobe analysis.

The Wabar samples were run in two separate irradiations. The INAA analyses were performed using the standard procedures of the Johnson Space Center INAA lab as described by Mittlefehldt and Lindstrom (1991). In addition to those procedures, we analyzed for Au and Ir using South African Bureau of Standards SARM-7 platinum ore as the standard. Subsequent to our analyses, we discovered that SARM-7 is inhomogeneous on the scale of our typical sample size (*i.e.*, 50 mg) and that the recommended Au concentration is about 2 times too high. We have subsequently back calibrated the SARM-7 samples used in the irradiations for the Wabar samples against U.S. National Museum standard Allende. Uncertainties in the INAA data are as follows: <3%—Na, Fe, Sc, Cr, Co, Ni, La, Ce, Sm and Hf; 3–7%—K, Ba, Eu, Yb, Lu and Th; 7–10%—Cs; 10–20%—Ca, Rb, Tb, Zr, Ta and U; 30–40%—Nd. The uncertainties in As and Sb are quite variable and are 15–40% and 10–30%, respectively. Iridium and Au are special cases because of the uncertainties involved in the standard; the Au and Ir data are considered to be accurate to ~20%. The precision of the data for these elements is ~3–5% for Ir and ~20% for Au. The Wabar and Nejed meteorite samples were analyzed at UCLA using their standard INAA procedures for iron meteorites (Wasson *et al.*, 1989).

Throughout this report the term "large" will refer to specimens >1 mm in diameter from which we could generate physical splits for optical, electron-microprobe and INAA analyses. The term "small" refers to those beads <1 mm in diameter which were analyzed as a group by INAA first, followed by thin sectioning, optical studies and microprobe

analysis of the activated samples. In addition, the terms "melt-spray" and "beads" are used synonymously.

PETROGRAPHIC DESCRIPTIONS

The most notable difference between the massive Wabar melts and the fine-grained melt-spray (see Fig. 1 and compare with the Fig. 2 of Hörz *et al.*, 1989) is the substantially increased homogeneity of the latter at optical scales. In thin-section, the beads are generally of uniform color that ranges from dark brown to yellowish tan. Schlieren are present in most beads, but are much more diffuse and subtle in comparison to those found in the black and white melts. Some rare beads lack schlieren and are truly optically homogeneous.

Finely disseminated Fe-Ni spherules, abundant in the black and white melts (*e.g.*, Brett, 1967; Gibbons *et al.*, 1976), are almost totally absent in the melt beads. In addition, the beads possess a much lower degree of vesicularity compared to the black and white melts. Vesicularity, when present, is generally confined to a small number of large vesicles within the beads. Some exceptionally large vesicles may approach the scale of the beads themselves. Clastic debris is virtually absent in the holohyaline interiors of the beads, yet it can be abundant on the exterior surfaces; objects >5 mm in size invariably seem to possess dusty coatings. A white, glassy clast formed the core of one broken-dumbbell sample.

Cumulatively, the petrographic observations suggest that the melt volume from which the beads were derived was hotter than that which gave rise to the massive black and white melts.

ANALYTICAL RESULTS

Elemental concentrations for individual melt samples are listed in Tables 1*a–c* and separated into small and large specimens. Typically, for a given sample 20–40 electron-microprobe spot analyses were averaged to yield the major-element composition for that sample. Table 2 summarizes the new analyses by presenting calculated averages (microprobe) or measured bulk values (INAA) of small and large melt particles, as well as the newly measured bulk compositions of the Wabar and Nejed meteorites. For comparison, the average compositions of the black and white melts, along with our best estimate of the Wabar target composition (from Hörz *et al.*, 1989) are also presented in Table 2. We discovered a systematic error in the data-reduction routine for the electron-microprobe concentrations of Ni reported in Hörz *et al.* (1989), and the corrected values are reported here. We have also recalculated Ir and Au concentrations for samples reported by Hörz *et al.* (1989) and report these corrected data in Table 2. Note the generally good agreement between microprobe and INAA results for those elements determined by both techniques.

Previously, Morgan *et al.* (1975) analyzed two "impactites" and a glass coating from a shocked clast from Wabar Crater. It is difficult to directly compare our results with theirs because Morgan *et al.* did not present petrographic details for their samples. Nonetheless, their Ni (1330–6600 ppm), Ir (87–740 ppb) and Au (3.4–37 ppb) data agree well with the range we have determined for ballistically dispersed glasses (Tables 1*b,c*).

The salient compositional trends of all Wabar materials analyzed are summarized in graphical form in Fig. 2. The connecting lines of major siderophile elements are intended to portray the mixing and dilution of a quartz-rich target with a group

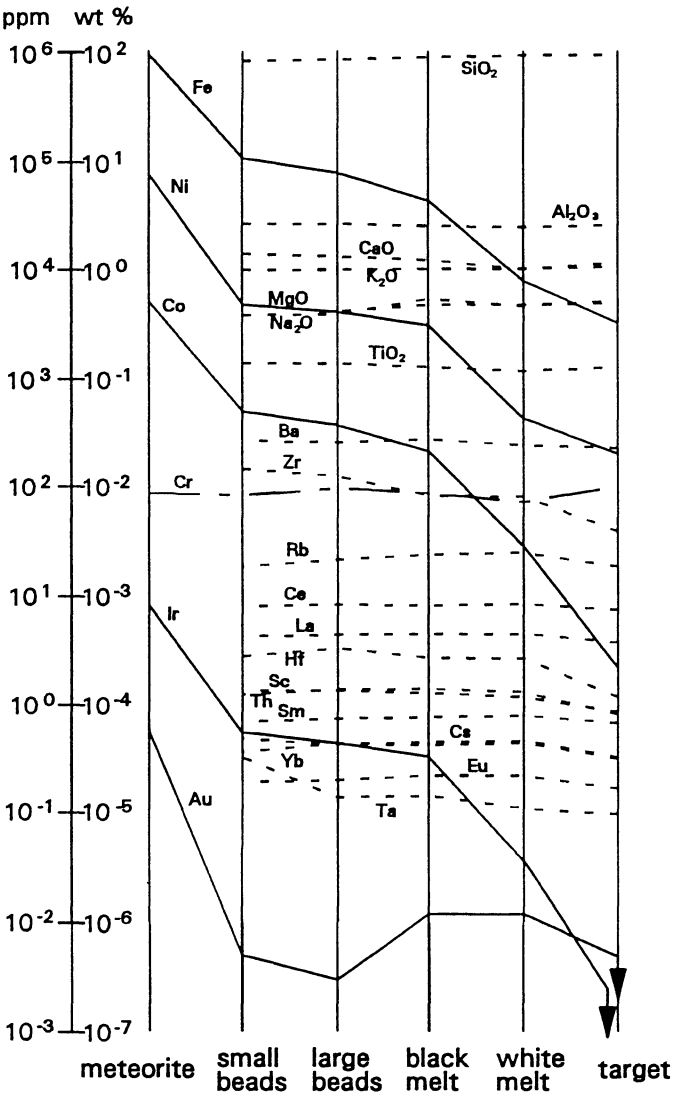

FIG. 2. Average concentrations of major-, minor- and select trace-elements in various glasses and their progenitors from Wabar. Data from Table 2. Solid lines—elements derived predominantly from the meteorite; dashed lines—elements derived from the target. Cr is in about the same concentration in impactor and target.

IIIA iron impactor. Perfect mixing would yield parallel slopes among all elements, regardless of absolute concentration. Because the slopes differ, elemental fractionation must have occurred. The major purpose of Fig. 2 is to illustrate that the Wabar melts cannot be simple mixtures of the projectile and target lithologies.

DISCUSSION

All melt samples are enriched in meteorite-derived siderophiles, some by substantial amounts. The Fe- and Ni-concentrations of the various melts are shown in Fig. 3; the dashed line labelled "m" represents the Fe/Ni ratio of the Wabar meteorite. Because of the low Fe- and Ni-concentrations within the target rock (Table 2), the high concentrations of these elements in the melt samples could only have been derived from the Wabar projectile. Figure 3a displays the (corrected) micro-

TABLE 1*a*. Average electron-microprobe analyses (in wt%) for four small (<1 mm) glass bead samples.

	MB17	MB18	MB19	DB20†
SiO_2	80.4	79.4	83.1	79.6
TiO_2	0.10	0.10	0.21	0.10
Al_2O_3	2.51	2.50	2.89	2.56
Cr_2O_3	0.01	0.01	0.02	0.01
Fe*	10.8	11.6	6.10	11.2
Ni*	0.47	0.53	1.07	0.44
MnO	0.01	0.01	0.01	
MgO	0.33	0.33	0.80	0.34
CaO	1.01	1.00	2.48	1.04
Na_2O	0.33	0.33	0.50	0.34
K_2O	0.95	0.94	1.09	0.95
sum*	100.2	100.2	100.3	99.9

Approximately 40 individual spot analyses were averaged for each bead.
* Fe and Ni reported as elements to facilitate comparison with data on the Wabar and Nejed meteorites (Table 2). The sum includes Fe and Ni as oxides.
† Sample 4 (DB20) was a dumbbell-shaped particle (see Fig. 1c).

probe data for the black and white melts from Hörz *et al.* (1989), while the new microprobe analyses on the various-sized glass beads are illustrated in Fig. 3b. The averaged microprobe data and INAA data for the Wabar melt samples (Tables 1*a–c*) can be seen in Fig. 3c.

In comparing the data from these plots, three trends seem significant:

1) The concentration of siderophiles within the large and small glass beads is substantially higher than in the black and white melts. Although there is considerable overlap in the spot analyses, the white melts never exceed 3% Fe and 0.3% Ni, while the black melts never exceed 9% Fe and 0.5% Ni (Fig. 3a). High siderophile concentrations are common among the large and small glass beads, however, and many possess average Fe-concentrations of >10% (Fig. 3b,c). Figure 3c illustrates that the small (<1 mm) glass beads generally exhibit higher siderophile contents than the large (>1 mm) beads, which, in turn, exhibit substantially higher Fe- and Ni-concentrations than the average black melt. Using the average major element compositions listed in Table 2, the following approximate amounts of Wabar meteorite were added to Wabar sandstone: 0.4% for the white melt, ~4% for the black melt, ~7% for the large glass beads and ~11% for the small glass beads. The latter numbers represent exceptionally high meteoritic contamination compared to both terrestrial and lunar impact melts (*e.g.*, Morgan *et al.*, 1975; Palme *et al.*, 1978) and are exceeded only by glasses from Meteor Crater (Mittlefehldt *et al.*, 1992).

2) There is large scatter in the Fe/Ni ratios from 4 to 40 for the individual microprobe analyses, while the Wabar meteorite possesses an Fe/Ni ratio of 12.4. This indicates substantial fractionation of Fe relative to Ni in the glass. The Wabar meteorite has a mean taenite bandwidth of 0.95 mm (Buchwald, 1975); approximately the same size scale as the small glass beads we analyzed. Therefore, heterogeneous distribution of taenite and kamacite in the glass might cause some of the observed Fe/Ni fractionation. Gibbons *et al.* (1976) measured Fe/Ni ratios in Wabar taenite of 2.3 and in kamacite of 13.4 (dashed lines labelled "k" and "t" in Fig. 3). Hence, Fe/Ni ratios in the glass as low as 4 might be caused by dissolution of taenite in the glass. However, Fe/Ni ratios as high as 40 cannot be obtained from kamacite (Fig. 3) and inhomogeneous dissolution of taenite and kamacite in the glasses cannot explain the entire range in Fe/Ni ratios observed. This is similar to the conclusions of Brett (1967) and Gibbons *et al.* (1976) who predominantly analyzed the metal-rich, opaque droplets. We conclude that individual melt volumes possess highly variable and fractionated siderophile element contents on the scale of micrometers. The most Ni-rich group in Fig. 3b represents analyses of a single, small glass bead that has an average Ni-content of ~1%, nearly twice as much as the next most Ni-rich sample and 3 to 4 times higher than most average Wabar glass samples (see Fig. 3c).

3) Compared to the Wabar octahedrite, all Wabar melts are generally depleted in Ni relative to Fe, as evidenced by the individual- and bulk-glass analyses. The glass microprobe averages are not systematically lower than the INAA bulk analyses, indicating that most meteoritic contamination resides in the glass and that the opaques play only a minor role. Hence, although Ni-rich opaques are described by Brett (1967) and Gibbons *et al.* (1976) in the black melt, similar opaques are not a significant host for siderophile elements in the ballistically dispersed glasses. A proper mass balance between opaques and glasses is not readily accomplished here, as modal abundance data of opaques in glass are not available, and we do not know the abundances of the different glass types. In thin section the opaques compose ≪1% of the sample and seem to be modally insufficient to compensate for the observed Ni-deficiency in the various glasses.

The INAA bulk analyses indicate that the black and white melts have Fe/Ni ratios, corrected for contributions from the target rock, that are greater by a factor of ~1.1 compared to the Wabar meteorite. The large and small glass beads have ratios that are greater by factors of 1.5 and 1.8, respectively. Thus, Ni-depletion (or Fe-enrichment) intensifies systematically with increasing siderophile element concentration in the various Wabar melts. The siderophile element contents seem dependent on bead size as well; the small glass beads generally have higher

TABLE 1*b*. INAA analyses for 16 individual small (<1 mm) glass bead samples.

	MB1	MB2	MB3	MB4	MB5	MB6	MB7	MB8
Sc	1.15	1.13	1.10	1.13	1.30	1.15	1.24	1.14
Cr	75	83	86	82	93	73	83	90
Fe	9.43	11.6	10.8	10.1	6.68	11.4	14.0	10.3
Co	516	527	532	450	309	500	571	472
Ni	5580	5380	5780	4010	3160	3890	4300	4580
Ir	500	540	730	570	420	400	120	670

Data are in ppm except Fe (wt%) and Ir (ppb).
INAA data for the grouped small beads (see text) are presented in Table 2.

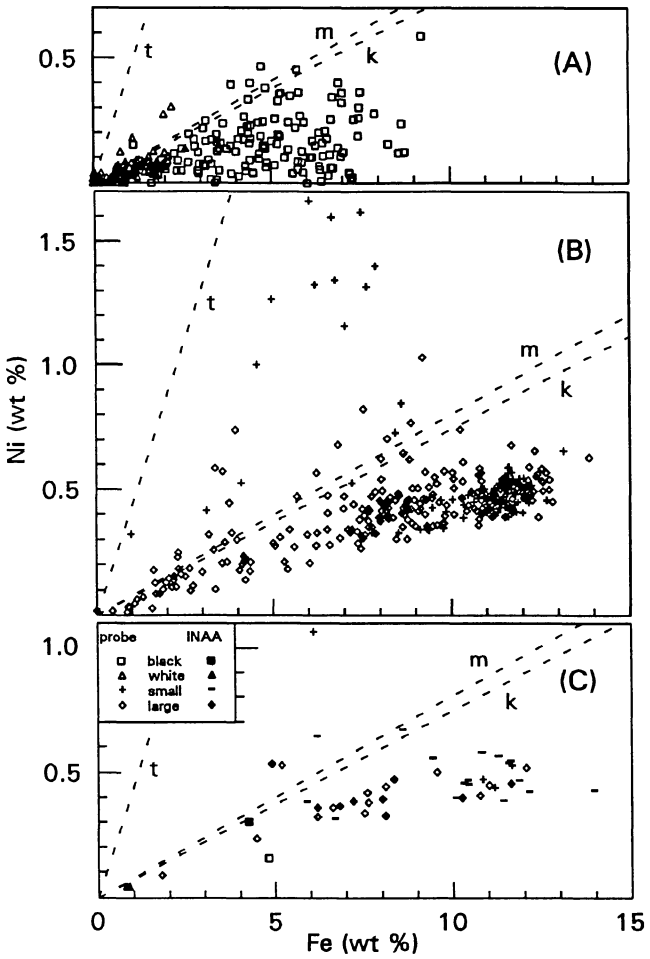

FIG. 3. Fe- and Ni-concentrations in various Wabar glasses compared to the bulk meteorite, kamacite and taenite Fe/Ni ratios (dashed lines labelled "m", "k" and "t," respectively) of the Wabar meteorite. Kamacite and taenite data from Gibbons *et al.* (1976). (a) Individual electron-microprobe spot analyses of black and white melts from Hörz *et al.* (1989) using corrected Ni-values (see text). (b) Individual electron-microprobe spot analyses of the large and small melt beads. The most Ni-rich points (>1%) are all from one sample. (c) Averaged electron-microprobe data and measured INAA bulk compositions of Wabar glasses. Symbols legend in part c applies to all parts.

concentrations than the larger glass beads, which have higher concentrations than the massive black melts. The trend of increasing Ni-depletion follows the petrographic evidence of increased melt homogeneity and inferred thermal history: the hottest Wabar melts are those most contaminated with siderophiles

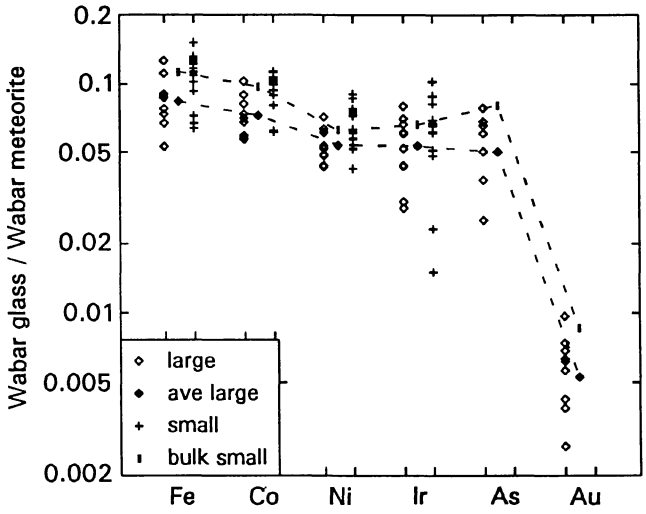

FIG. 4. Siderophile element concentrations relative to the Wabar meteorite for individual glass beads obtained by INAA. Dashed lines connect bulk small beads (upper line) or average large bead (lower line).

and these contaminants have the highest Fe/Ni ratios. Because of this, we believe that the fractionation of the siderophiles was caused by some vapor-fractionation process which is ill-defined at present.

Figure 4 depicts the siderophile element concentrations of individual glass beads normalized to those of the Wabar meteorite. Relative to Fe, Co seems to be present in approximately meteoritic proportions, while Ni, Ir and As are slightly depleted to similar abundances. Gold is severely depleted, with average Fe/Au ratios of 15.7× and 13.1× Wabar meteorite for the large and small beads, respectively. Note that Ir, the most refractory element (Scott, 1972), shows similar depletion to As, the most volatile. The relative depletion sequence of siderophiles is unrelated to vapor pressure at ambient conditions, which seems to argue against a simple vapor-fractionation process as the cause of the observed abundance of siderophile elements.

The relative depletion sequence illustrated for Wabar in Fig. 4 is qualitatively similar to that observed at the Henbury and Wolfe Creek Craters, Australia (Attrep *et al.*, 1991). The latter structures, like Wabar, exhibit well-preserved glass and projectile specimens. Among the siderophile element data available for all three craters, Co is the least depleted species in these Australian structures as well, followed by Ni, Ir and Au. At Wolfe Creek and Henbury craters, however, Ir is much more depleted in the glasses relative to Co (Attrep *et al.*, 1991) than it is in the Wabar glasses.

TABLE 1*b*. Continued.

MB9	MB10	MB11	MB12	MB13	MB14	MB15	MB16
1.15	1.11	1.15	1.14	1.96	1.08	1.20	1.22
82	82	84	80	128	65	83	75
11.6	11.3	10.4	8.60	5.88	6.19	11.9	12.1
564	534	507	474	131	404	530	537
5450	5660	4540	6710	3850	6450	4690	4250
840	500	550	500	420	190	500	550

TABLE 1*c*. Electron-microprobe and INAA data for the large (>1 mm) glass bead samples.

	LB 3A1	LB 3A2	LB 3B	LB 3C	LB 3D	LB 3E	LB 4A	LB 4B	LB 4C	LB 4D	LB 5A	LB 5B	LB 5C
Electron-microprobe													
SiO_2	85.6		80.4	93.0	84.2	84.3	81.2	85.1	84.5	87.8	80.2	79.0	83.7
TiO_2	0.12		0.11	0.18	0.11	0.13	0.11	0.16	0.13	0.15	0.11	0.10	0.13
Al_2O_3	2.75		2.52	2.15	2.69	2.65	2.47	2.99	2.59	2.72	2.55	2.50	2.90
Cr_2O_3	0.01		0.02	0.01	0.01	0.02	0.02	0.02	0.01	0.02	0.01	0.02	0.02
Fe*	6.61		10.8	1.80	8.11	7.62	9.54	5.18	7.51	4.48	11.0	12.0	7.59
Ni*	0.36		0.41	0.09	0.44	0.38	0.50	0.53	0.34	0.23	0.45	0.52	0.42
MnO	0.01			0.01	0.01	0.01	0.01	0.01	0.01	0.01	0.01	0.01	0.01
MgO	0.42		0.33	0.40	0.45	0.38	0.33	0.48	0.35	0.42	0.34	0.32	0.42
CaO	1.45		1.02	1.64	1.32	1.27	1.04	1.94	1.14	1.51	1.05	0.96	1.46
Na_2O	0.41		0.35	0.38	0.43	0.40	0.34	0.48	0.36	0.39	0.36	0.32	0.41
K_2O	1.01		0.95	0.81	1.04	1.01	0.95	1.14	0.98	1.03	0.95	0.93	1.07
sum*	100.7		100.1	101.0	101.2	100.5	99.3	99.7	100.2	100.1	100.3	100.3	100.4
INAA													
Na_2O	0.396	0.413	0.384	0.406	0.414		0.371	0.473	0.365		0.337	0.333	
K_2O	0.87	0.89	0.91	0.92	0.95		0.88	0.97	0.86		0.85	0.95	
CaO	1.3	1.17	1.2	1.1	1.1		0.9	1.4	1.1		0.9	0.9	
Sc	1.30	1.27	1.35	1.44	1.33		1.18	1.54	1.23		1.11	1.17	
Cr	98	96	101	115	93		99	111	79		85	86	
Fe	6.20	7.20	8.10	8.02	6.20		8.34	4.90	6.82		10.2	11.6	
Co	289	341	357	372	298		411	297	341		451	516	
Ni	3220	3860	3270	3940	3600		4720	5320	3660		3990	4550	
As	0.24	0.26	0.20	0.31	0.26			0.27	0.10		0.15		
Rb	20	20	21	20	21		20	22	19		22	18	
Zr	150	110	110	140	90		100	180	100		130	100	
Sb	0.05	0.07	0.04	0.06	0.04		0.04	0.08	0.04				
Cs	0.38	0.44	0.39	0.42	0.42		0.38	0.42	0.36		0.45	0.34	
Ba	244	285	270	240	260		260	230	240		240	270	
La	4.83	4.16	4.63	4.61	4.50		4	4.52	4.39		4.13	4.36	
Ce	8.5	8.39	8.70	9.0	8.3		7.8	8.6	8.4		7.7	8.0	
Nd	5		5	4	4		4		5				
Sm	0.72	0.70	0.78	0.79	0.76		0.67	0.78	0.73		0.68	0.72	
Eu	0.19	0.19	0.21	0.20	0.20		0.19	0.19	0.19		0.18	0.19	
Tb	0.08	0.12	0.10	0.12	0.09			0.09	0.07		0.08		
Yb	0.40	0.43	0.43	0.52	0.43		0.38	0.47	0.38		0.37	0.41	
Lu	0.060	0.070	0.065	0.081	0.065		0.057	0.074	0.063		0.042	0.065	
Hf	3.57	2.75	3.08	3.62	2.78		2.71	4.83	3.37		2.50	2.69	
Ta	0.13	0.12	0.15	0.15	0.15		0.11	0.15	0.14		0.13	0.11	
Ir	430	500	360	500	360		540	250	234		650	580	
Au	3	4	2	2	4		2	4	6		4	<3	
Th	1.39	1.29	1.39	1.41	1.22		1.02	1.51	1.62		1.06	1.34	
U	0.40	0.42	0.40	0.50	0.38		0.39	0.56	0.37		0.32	0.38	

Electron-microprobe data in wt%, INAA data in ppm except Na_2O, K_2O, CaO and Fe in wt%; Ir and Au in ppb.
* Fe and Ni reported as elements to facilitate comparison with data on the Wabar and Nejed meteorites (Table 2). The sum includes Fe and Ni as oxides.

TABLE 2. Electron-microprobe and INAA data for various Wabar materials.

	Target+	White+ glass	Black+ glass	Large* beads	Small* beads	Wabar±	Nejed±
SiO_2	93.6	93.0	87.9	84.1	80.6		
TiO_2	0.12	0.11	0.12	0.13	0.13		
Al_2O_3	2.56	2.45	2.50	2.62	2.62		
Cr_2O_3	0.02			0.02	0.01		
Fe	0.32	0.60	4.14	4.53	9.94		
MnO	0.01	0.01	0.01	0.01	0.01		
MgO	0.47	0.45	0.45	0.39	0.45		
CaO	1.16	1.01	1.22	1.32	1.38		
Na_2O	0.52	0.46	0.54	0.39	0.38		
K_2O	1.06	1.02	1.02	0.99	0.98		
P_2O_5	0.02	0.01	0.01				
Na_2O	0.33	0.42	0.43	0.39	0.365		
K_2O	0.68	0.86	0.88	0.90	0.86		
CaO	0.49	0.72	0.73	1.12	0.80		
Sc	0.83	1.23	1.31	1.29	1.16		
Cr	78	73	87	96	83	65	110
Fe	0.25	0.79	4.25	7.77	10.4	91.5	91.7
Co	2	28	211	367	491	5000	4990
Ni	44	430	3040	4010	4700	74,600	73,000
Cu						170	164
Ga						18.1	18.6
As			0.40	0.20	0.32	3.85	4.0
Rb	18	24	23	20	18		
Zr	40	80	80	120	140		
Sb		0.12	0.06	0.05	0.05		
Cs	0.33	0.44	0.42	0.40	0.45		
Ba	230	240	270	250	270		
La	3.8	4.45	4.46	4.4	4.19		
Ce	7.5	8.4	8.1	8.3	8.1		
Nd	3.6	4.1	3.5	4.6			
Sm	0.70	0.79	0.76	0.73	0.68		
Eu	0.17	0.21	0.21	0.19	0.18		
Tb	0.11	0.09	0.08	0.09			
Yb	0.32	0.43	0.41	0.42	0.35		
Lu	0.05	0.067	0.060	0.06	0.055		
Hf	1.2	2.59	2.61	3.2	2.65		
Ta	0.10	0.11	0.14	0.13	0.31		
W						1.18	1.19
Re						850	850
Ir	<2	36	330	440	550	8150	8120
Pt						12.8	13.3
Au	<5	12	12	3	5	540	580
Th	0.86	1.17	1.28	1.33	1.33		
U	0.45	0.45	0.40	0.41	0.40		

Oxides and Fe in wt%; Re, Ir and Au in ppb; all other data in ppm.
For the average small bead, INAA data for the 16 grouped beads are shown (see text for details).
+ Compositions for the target, white glass and black glass are from Hörz *et al.*, 1989.
* Large beads and small beads represent averaged microprobe data or INAA data.
± Analysis of Wabar and Nejed meteorites provided by J. T. Wasson.

Conflicting evidence regarding a vapor-fractionation process seems to emerge from our analyses. On the one hand, the most fractionated materials are found in the smallest objects that have the largest specific free-surface areas, yet the relative sequence of depletion for specific elements does not correlate with vapor pressure, heat of vaporization or fusion, nor with any of a wide variety of other thermodynamic parameters that we explored, including ionic radii (Engelhardt *et al.*, 1987).

We considered the possibility that a chemically heterogeneous (on a cm scale) projectile produced the scatter and fractionation of siderophile element ratios in the Wabar glass samples. Figure 5 compares the CI-normalized Ni/Co and Ir/Co ratios for the various glasses with the Wabar and Cape York irons. Cape York is a large (57 ton) IIIA iron found as several individual masses in Greenland. Esbensen *et al.* (1982) analyzed a suite of Cape York samples and found chemical heterogeneity in this large iron meteorite. Their data (Fig. 5) show a clear magmatic signature with a slightly increasing Ni/Co ratio as the Ir/Co ratio decreases (Scott, 1972). We would expect any initial chemical heterogeneity in the pre-atmospheric Wabar mass similarly to have been caused by magmatic fractionation in the core of an asteroid and to exhibit an element-fractionation trend as indicated by the dashed line in Fig. 5. The Wabar glass samples do not display a magmatic trend and show a Ni/Co fractionation that is unlikely to have occurred on the IIIAB iron parent body. Also shown in Fig. 5 is a mixing line between kamacite (k) and taenite (off scale in figure). Although Ir/Co ratios for Wabar glasses are similar to that we estimate for kamacite, the Ni/Co

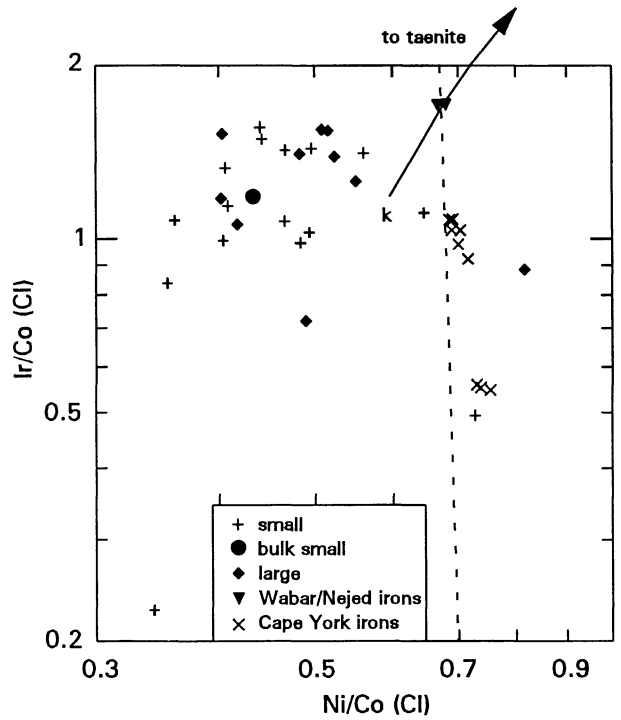

FIG. 5. Ni/Co and Ir/Co ratios in individual Wabar melt beads compared with those of Wabar and from a number of Cape York subsplits reported by Esbensen *et al.* (1982). The dashed line is a model fractional crystallization trend for Wabar. The solid line connects kamacite (k in figure) with taenite (off scale on figure). Ni and Co data for kamacite and taenite were taken from Gibbons *et al.* (1976). Ir in kamacite and taenite were estimated from bulk meteorite data (Table 2) and partitioning data for Cape York IIIA iron from Rasmussen *et al.* (1988).

ratios are systematically lower in the glasses. Hence, we see no evidence that the siderophile element fractionations observed in the Wabar glasses could have been inherited from a compositionally heterogeneous Wabar meteorite.

Dissemination of the Projectile

The concentration of siderophiles in the glasses may vary on both macroscopic and microscopic scales. The distinction between small and large beads at 1 mm is entirely arbitrary, yet we find a distinct trend of increasing meteorite content with decreasing melt-particle size, as well as with the color of the glass (*i.e.*, the white melts exhibit the lowest meteoritic contamination, followed by the black melts and then the smallest ballistic particles). This siderophile enrichment follows systematic trends in petrographic criteria that relate to melt temperature, such as clast-content, the frequency and crispness of schlieren, and the abundance of discrete Fe-Ni spheres.

The temperature of the impact melt is closely related to the decay profile of a propagating shock front. The highest temperatures are produced in the highest stratigraphic position in the target, at or close to the projectile-target interface. This is also the region where the impactor is heated to its peak temperature (*e.g.*, Ahrens and O'Keefe, 1977) and where deformation of the projectile is the greatest, leading to the largest contact area between projectile and target. These conditions are the most conducive to dissemination of relatively large amounts of impactor material into the relatively small melt volumes that will exist at this stage of crater development (*e.g.*, Gault *et al.*, 1968; Stöffler *et al.*, 1975). We interpret the evidence for elevated melt temperature and elevated siderophile element contents as an indication for a shallow stratigraphic position for the target material that formed the ballistic melt-spray. This is also consistent with the general material flow during cratering. Ballistic ejecta is believed to be derived from a shallower stratigraphic position than other displaced materials (*e.g.*, Maxwell, 1977). Following these arguments, the massive black and white melts would have been derived from successively deeper strata as previously postulated (Hörz *et al.*, 1989). Our results suggest that the amount of projectile material incorporated into impact melts may be sensitively related to the stratigraphic position within a crater's melt zone.

Fractionation of the Projectile

We have not found a simple explanation for the observed fractionation trends of siderophile elements in the Wabar glasses. Gibbons *et al.* (1976) present a good summary of possible fractionation processes, to which ionic radius controlled mobility of specific elements (Engelhardt *et al.*, 1987) must be added. The depletion trends illustrated in Fig. 4 tend to eliminate simple vapor fractionation of pure elements. The 1 bar boiling point of Ir (4701 K) is well above those of Co, Ni, Fe, Au (3201–3130 K) and especially As (875 K) (Robie *et al.*, 1978), yet Ir is more depleted than Co and Fe, and similarly depleted as Ni and As. Similarly, vapor fractionation of oxides (*e.g.*, Walter and Giutronich, 1967; King, 1982) seems unlikely, as IrO_2 dissociates to metal plus oxygen at 1373 K and should then be refractory, while As_2O_3 sublimates at 466 K (Weast *et al.*, 1985). However, we cannot determine the chemical state of the siderophile elements during the impact process and therefore cannot rigorously test vapor-fractionation scenarios. Brett (1967) and Gibbons *et al.* (1976) also argued against vapor fractionation and invoked selective oxidation to explain the compositional trends of the Fe-Ni spherules in the Wabar melts. While selective oxidation may have indeed been responsible for the compositional trends observed in the metal spheres, it can only be part of the whole story. The observed fractionations of bulk glass must have been produced by a different process. The depletion trends illustrated in Fig. 4 are based on bulk analyses of the most meteorite-rich specimens, yet the trends indicated also apply to the black and white melts as deduced from Fig. 3 and Table 2. Not only are pure glass (averaged microprobe analyses) and bulk samples (INAA) rather similar in composition, but both materials strongly indicate absolute loss of some elements derived from the impactor. The siderophile element abundances in the Wabar glasses strongly suggest that an open system was functional during the cratering process.

The strong fractionations observed for siderophile elements in the glass beads are not observed for lithophile elements. Figure 6 shows selected lithophile elements in the glass beads normalized to an average of shocked clasts from the black and white melts (A) and the drift sand (B) (Hörz *et al.*, 1989). Lithophile elements, from the relatively volatile alkali elements to the refractory rare-earth elements, show no evidence for selective vapor fractionation when compared to the clast samples. The slight variations that are observed are plausibly due to variations in the target lithology. For example, the overabundance of Ca in the glass compared to the clasts (Fig. 6*a*) may

reflect calcite cement or caliche in the near surface, while enhanced K may indicate an additional K-feldspar component. The glass beads are enriched in lithophiles by a factor of 2–4 compared to the modern drift sand (Fig. 6*b*), probably because fine dust, the likely source for much of the lithophile trace elements, is winnowed out of the sand while drifting. Hence, the target materials were barely affected by fractionation, if at all. We take this observation to imply that siderophile element fractionation did not occur during the physical dissemination of impactor material, but that fractionation was substantially completed before intimate mixing of impactor residue and target melts commenced. Fractionation seems to be confined to the projectile and must have occurred while the meteorite was still separated from the target melts.

During cratering, the time scales required to compress and heat the projectile are short compared to the time scale of crater growth (Ahrens and O'Keefe, 1977; Cintala, 1991; Orphal, 1977). Decompression of the projectile will occur at times when substantial fractions of the crater are still under compression. Projectile decompression entails substantial disruption of the impactor, creating a large free surface and facilitating vaporization and ionization of impactor material. Fractionation processes are most likely to occur during this time period as the hot, decompressed impactor has a large free surface area. The fractionated impactor residues will then be incorporated into the target melts as the target material decompresses, expands and accelerates to set up the macroscopic flow field of the crater. The selective oxidation suggested by Brett (1967) and Gibbons *et al.* (1976) must be a relatively late process superimposed on early fractionations of the penetrating impactor.

The depletion factors for the siderophile elements illustrated in Fig. 4 indicate the relative fraction of each element that has escaped the system. Because we feel confident that we have a representative suite of Wabar materials, we conclude that physical loss of these elements must have been to the atmosphere by vaporization. While the relative volatilities of some elements analyzed (*e.g.*, Ir) seem at odds with this conclusion, we suggest that the complex physical and chemical processes occurring during the short impact event preclude detailed testing of any fractionation models. Walter and Giutronich (1967) and Walter (1967) demonstrated reversals in relative volatility for SiO_2-rich systems thought to be the progenitors of tektites. We suggest that similar effects could govern the vaporization of the Wabar projectile.

Throughout this report we have described siderophile element depletion relative to Fe, a procedure that tacitly assumes that Fe was the least affected species; this assumption seems justified on the basis of Fig. 4. However, the data and information presently in hand do not permit an assessment of the quantity of Fe that may have been lost to the atmosphere, if any. Such an evaluation requires accurate modal-abundance data of the major glass-types for mass-balance purposes. In the absence of such data, we can neither calculate the absolute fraction of meteorite residue contained in these glasses, nor the quantity that may have been lost.

CONCLUSIONS

The major conclusions that can be made following our examination of the various glass samples from the Wabar impact structure, Saudi Arabia are:

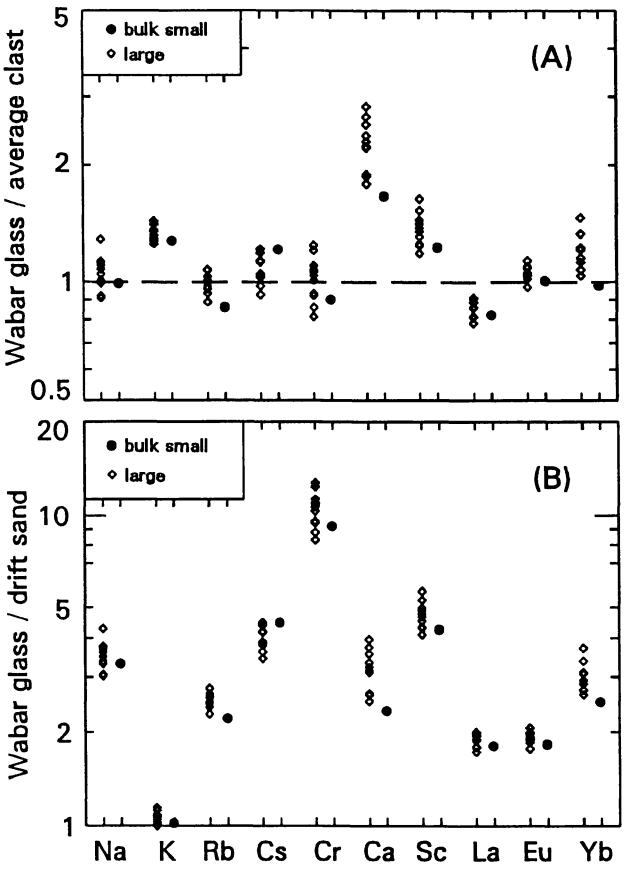

FIG. 6. Comparison of lithophile elements of varying volatility in Wabar glass beads (this study) with (a) an average of Wabar clasts, and (b) modern Wabar drift sand from Hörz *et al.* (1989).

1) The ballistically dispersed melts from Wabar Crater are petrographically and chemically more homogeneous than the massive melts. Compared to the massive melts, the ballistically dispersed melts contain fewer and less distinct schlieren, much less clastic debris, very few vesicles, and almost no Fe-Ni spherules.

2) Siderophile element abundances in the ballistically dispersed glasses are fractionated relative to the Wabar meteorite. The siderophile element depletions are not easily correlated with any physical or chemical property of the elements.

3) Siderophile element concentrations are highest in the smallest glass beads and lowest in the massive melts. The meteoritic component of the ballistically dispersed glasses is commonly $>10\%$, while the massive melts generally contain $<5\%$ meteoritic material.

4) Lithophile element abundances in the ballistically dispersed glasses are not fractionated relative to the target materials. Slight variations in the lithophile element abundances are explainable as arising from heterogeneity in the target material.

5) Based on our data and models for crater forming processes, we posit that the ballistically-dispersed glasses were formed from material at shallow levels in the target zone where temperatures were higher and more intimate physical contact with the disrupting impactor was achieved. Siderophile element fractionations were produced early, while the impactor was undergoing decompression and prior to mixing with the target glasses.

While we cannot readily explain the fractionation process(es) that produced the impactor residues at the Wabar Crater, we feel confident that mixing with, and dissolution of siderophile elements into the target melts occurred after the siderophile element fractionation was substantially completed. Furthermore, the absolute amount of projectile material mixed into the melt is sensitively related to stratigraphic position within the evolving melt zone at Wabar; greater quantities of siderophile elements are mixed into the higher stratigraphic levels.

We have no reliable basis for extrapolation of these findings from the 90-m diameter Wabar structure to larger impacts, especially those at multi-ring basin scales. We appreciate that the abundance of siderophile elements is central to a number of ongoing, fundamental debates such as the K-T boundary catastrophe, the identification of pristine lunar lithologies and the compositions of massive impactors throughout geologic history. Nevertheless, direct extrapolation and application of the Wabar data to giant impacts seems speculative beyond justification at present. What must be learned from the Wabar observations, in complete agreement with Attrep *et al.* (1991), is that great care is needed in assigning specific projectile types and associated masses to individual impact craters without detailed knowledge of possible fractionation processes and effects. Some of these issues seem amenable to experimental inquiry and clarification.

Acknowledgements—R. Clarke and K. Fredriksson, Smithsonian Institution, Washington, D. C., generously provided all samples investigated in this study and J. Wasson, UCLA, was kind enough to analyze the Wabar and Nejed meteorite specimens. Reviews of an early version of this manuscript by M. Cintala and J. H. Jones, and formal reviews by R. Brett, L. S. Walter and an anonymous reviewer are greatly appreciated.

Editorial handling: R. A. F. Grieve.

REFERENCES

Ahrens T. J. and O'Keefe J. D. (1977) Equations of state and impact-induced shock-wave attenuation on the Moon. In *Impact and Explosion Cratering* (eds. D. J. Roddy, R. O. Peppin and R. B. Merrill), pp. 639–658. Pergamon Press, New York, New York.

Attrep M., Jr., Orth C. J., Quintana L. R., Shoemaker C. S., Shoemaker E. M. and Taylor S. R. (1991) Chemical fractionation of siderophile elements in impactites from Australian meteorite craters (abstract). *Lunar Planet. Sci.* **22,** 39–40.

Brett R. (1967) Metallic spherules in impactite and tektite glasses. *Amer. Miner.* **52,** 721–733.

Buchwald V. F. (1975) *Handbook of Iron Meteorites.* Univ. Calif. Press, Berkeley, California. 1418 pp.

Cintala M. J. (1991) Impact-induced thermal effects in the lunar and mercurian regoliths. *J. Geophys. Res.* **97,** 947–973.

Ehmann W. D. (1962) The abundance of nickel in some natural glasses. *Geochim. Cosmochim. Acta* **26,** 489–493.

Engelhardt W. v., Luft E., Arndt J., Shock H. and Weiskirchner W. (1987) Origin of Moldavites. *Geochim. Cosmochim. Acta* **51,** 1425–1443.

Esbensen K. H., Buchwald V. F., Malvin D. J. and Wasson J. T. (1982) Systematic compositional variations in the Cape York iron meteorite. *Geochim. Cosmochim. Acta* **46,** 1913–1920.

Gault D. E., Quaide W. L. and Oberbeck V. R. (1968) Impact cratering mechanics and structures. In *Shock Metamorphism of Natural Materials* (eds. B. M. French and N. M. Short), pp. 87–100. Mono Book Corp., Baltimore, Maryland.

Gibbons R. V., Hörz F., Thompson T. and Brownlee D. E. (1976) Metal spherules in Wabar, Monturaqui, and Henbury impactites. *Proc. Lunar Sci. Conf.* **7th,** 863–880.

Grieve R. A. F. (1982) The record of impact on Earth: Implications for a major Cretaceous/Tertiary impact event. In *Geological Implications of Impacts of Large Asteroids and Comets on the Earth* (eds. L. T. Silver and P. H. Schultz), pp. 25–37. *Geol. Soc. Am., Spec. Pap.* **190,** Boulder, Colorado.

Holm D. A. (1962) New meteorite localities in the Rub' al Khali, Saudi Arabia. *Am. J. Sci.* **260,** 303–309.

Hörz F., See T. H., Murali A. V. and Blanchard D. P. (1989) Heterogeneous dissemination of projectile materials in the impact melts from Wabar Crater, Saudi Arabia. *Proc. Lunar Sci. Conf.* **19th,** 697–710.

King E. A. (1982) Refractory residues, condensates, and chondrules from solar furnace experiments (abstract). *Lunar Planet. Sci.* **13,** 389–390.

Maxwell D. E. (1977) Simple Z model of cratering, ejection, and the overturned flap. In *Impact and Explosion Cratering* (eds. D. J. Roddy, R. O. Peppin and R. B. Merrill), pp. 1003–1008. Pergamon Press, New York, New York.

Mittlefehldt D. W. and Lindstrom M. M. (1991) Generation of abnormal trace element abundances in Antarctic eucrites by weathering processes. *Geochim. Cosmochim. Acta* **55,** 77–87.

Mittlefehldt D. W., See T. H. and Hörz F. (1992) Projectile dissemination in impact melts from Meteor Crater, Arizona (abstract). *Lunar Planet. Sci.* **23,** 919–920.

Morgan J. W., Higuchi H., Ganapathy R. and Anders E. (1975) Meteoritic materials in four terrestrial meteorite craters. *Proc. Lunar Planet. Sci. Conf.* **6th,** 1609–1623.

Orphal D. L. (1977) Calculations of explosion catering—II. Cratering mechanics and phenomenology. In *Impact and Explosion Cratering* (eds. D. J. Roddy, R. O. Pepin and R. B. Merrill), pp. 907–917. Pergamon Press, New York, New York.

Palme H. (1982) Identification of projectiles of large terrestrial impact craters and some implications for the interpretation of Ir-rich Cretaceous/Tertiary boundary layers. In *Geological Implications of Impacts of Large Asteroids and Comets on the Earth* (eds. L. T. Silver and P. H. Schultz), pp. 223–234. *Geol. Soc. Am., Spec. Pap.* **190,** Boulder, Colorado.

Palme H., Janssens M.-J., Takahashi H., Anders E. and Hertogen J. (1978) Meteoritic material at five large impact craters. *Geochim. Cosmochim. Acta* **42,** 313–323.

Philby H. St. J. B. (1933) *The Empty Quarter.* H. Holt and Company. 364 pp. New York, New York.

Rasmussen K. L., Malvin D. J. and Wasson J. T. (1988) Trace element partitioning between taenite and kamacite; relationship to the cooling rates of iron meteorites. *Meteoritics* **23,** 107–112.

Robie R. A., Hemmingway B. S. and Fisher J. R. (1978) Thermodynamic properties of minerals and related substances at 298.15 K and 1 bar (10^5 Pascals) pressure and at higher temperatures. *U.S. Geol. Surv. Bull.* **1452,** 456 pp.

Scott E. R. D. (1972) Chemical fractionation in iron meteorites and its interpretation. *Geochim. Cosmochim. Acta* **36,** 1205–1236.

Spencer L. J. (1933a) Appendix A: Meteorites and fulgurites. In *The Empty Quarter.* H. Holt and Company. 365–370 pp.

Spencer L. J. (1933b) Meteoritic iron and silica-glass from meteorite craters of Henbury (central Australia) and Wabar (Arabia). *Mineral Mag.* **23,** 387–404.

Stöffler D., Gault D. E., Wedekind J. and Polkowski G. (1975) Experimental hypervelocity impact into quartz sand: Distribution and shock metamorphism of ejecta. *J. Geophys. Res.* **30,** 4062–4077.

Storzer D. and Wagner G. A. (1977) Fission track dating of meteorite impacts (abstract). *Meteoritics* **12,** 368–369.

Walter L. S. (1967) Tektite compositional trends and experimental vapor fractionation of silicates. *Geochim. Cosmochim. Acta* **31,** 2043–2063.

Walter L. S. and Giutronich J. E. (1967) Vapor fractionation of silicate melts at high temperatures and atmospheric pressure. *Solar Energy* **11,** 163–169.

Wasson J. T., Ouyang X., Wang J. and Jerde E. (1989) Chemical classification of iron meteorites: XI. Multi-element studies of 38 new irons and the high abundance of ungrouped irons from Antarctica. *Geochim. Cosmochim. Acta* **53,** 735–744.

Weast R. C., Astle M. J. and Beyer W. H. (1985) *CRC Handbook of Chemistry and Physics.* **66th Ed.** CRC Press, Cleveland, Ohio.